N93-15515

Effects of higher order aberrations on beam shape in an optical recording system

Mark S. Wang and Tom D. Milster
Optical Sciences Center, University of Arizona
Tucson, AZ 85721

Abstract

An unexpected irradiance pattern in the detector plane of an optical data storage system was observed. Through wavefront measurement and scalar diffraction modeling, we discovered that the energy redistribution is due to residual third-order and fifth-order spherical aberration of the objective lens and cover-plate assembly. The amount of residual aberration is small, and the beam focused on the disk would be considered diffraction limited by several criteria. Since the detector is not in the focal plane, even this small amount of aberration has a significant effect on the energy distribution. We show that the energy redistribution can adversely affect focus error signals, which are responsible for maintaining sub-micron spot diameters on the spinning disk.

PRECEDING PAGE BLANK NOT FILMED

In optical data storage systems, focusing and tracking servo controls are necessary to keep the micron-sized laser spot in focus and aligned with the proper track as the disk spins. Focusing and tracking error signals are commonly derived from the beam reflected from the optical disk[1]. The reflected beam exhibits a peak-to-peak wavefront deviation less than 0.25 wave and a rms deviation less than 0.07 wave, which is essentially diffraction limited. In our focus-error detection technique, the reflected beam is refocused by an auxiliary lens, and a detector is placed just outside of the auxiliary-lens focus[2]. The observed irradiance distribution on the detector plane is significantly different from that predicted by assuming that the beam has no aberration. The cause of this effect is mainly residual higher-order spherical aberration that redistributes the Gaussian beam energy into the caustic region. The energy redistribution can affect focus-error signals.

In this paper, we first present scalar diffraction modeling results of the reflected beam on the servo detector. Then we will show wavefront measurement results at various planes in the optical system. Finally, wavefront measurement and diffraction modeling are combined to explain our

experimental observation of the irradiance pattern at the focus-servo detector plane.

In Figure 1, the layout of the head optics is drawn in solid lines. The laser diode is a Sharp LT024 operating at 780 nm with beam divergences of 10° and 29° (FWHM) parallel and perpendicular to the junction, respectively. The laser diode output is collimated by a lens with a focal length of 6.25 mm and an aperture of 5.0 mm. The collimated beam is then circularized by an anamorphic prism pair with a magnification of 3x. The beam passes through a partially polarizing beam splitter (PPBS) and is focused onto the disk by an Olympus AV4350-3 objective lens mounted on TAOH-PB7 actuator. The objective lens is a glass triplet with designed rms aberration of $< 0.018\lambda$ on axis and $< 0.05\lambda$ at 100 μm field. The numerical aperture (NA) of the objective is 0.5 and the aperture diameter is 4.3 mm, which truncates the Gaussian beam profile at 0.76 of its $1/e^2$ width. The aperture of the objective lens is the stop for the optical system. The light reflected from the disk is re-collimated by the objective lens and directed to the detection optics by the PPBS. The equivalent air path length from the objective lens to the plano-convex detector lens is 150 mm. The

detector lens has a 124 mm focal length and focuses the light onto quad detector #2, which is 17.62 mm outside its focal plane.

A physical-optics analysis is accomplished through modeling the amplitude and phase of the laser beam's electric field[3]. Beam propagation is simulated through the use of Fresnel diffraction calculations[4]. In this model, a scalar diffraction approach is used. The beam is represented by a matrix of complex values, where each matrix element represents a different sample point in the wavefront. The complex values represent the amplitude and phase of the wavefront at the given point. Fresnel diffraction is computed with Fast Fourier Transforms (FFTs). Propagation of collimated beams between lenses is modeled using the angular spectrum method. Aberrations are represented by Zernike polynomials.

In our optical system there are several sources of aberration. The beam emitted from laser diode has astigmatism[5]. The collimating lens is carefully aligned to balance the laser diode astigmatism[6]. For light passing through, the prism pair and PPBS are just plane parallel plates that generate almost no aberration. The objective lens is designed to

compensate aberration caused by the disk cover glass, but it is not aberration free. Actually, the objective lens and cover plate are the main aberration sources in this system. Aberrations are induced when the beam is focused through the objective lens and as the beam is passed through the cover plate. When the beam is reflected back, odd aberrations are canceled and even aberrations are doubled. Another source of aberration is when the PPBS reflects light to detection optics. The reflecting surface generates astigmatism. The amount of aberration generated depends on the quality of the beam splitter. The detector lens and PBS have very little contribution to total aberration since they are used at very small NA.

In our model, aberrations are added in the entrance and exit pupil of the objective lens. Contributions of other components are traced back to either pupil. The amount of aberration refers to that of single pass.

We now discuss our modeling results. The beam is propagated from the collimating lens, through the objective lens, down to the disk, back through the objective lens, and to the detector plane. Line

profiles of the irradiance pattern at the detector plane are shown in Figure 2 for several situations. All the line profiles are normalized to the peak at the center. No aberration is present and the disk is in focus for Figure 2a. The edge of the intensity irradiance pattern decays like a Gaussian beam. The center shows diffraction rings caused by the stop. The beam profile is the image of Fresnel diffraction pattern in a plane 997 mm away from the detector lens, i.e., 847 mm from the stop. The stop size is 2.15 mm in radius, so the Fresnel number is:

$$\frac{r^2}{\lambda Z} = \frac{(2.15\times10^{-3})^2}{0.78\times10^{-6}\times0.847} = 7.0 \qquad (1)$$

The peak at the center is very clear. Figure 2b shows the line profile when -0.25 wave of balanced third-order spherical aberration is added at the objective pupil. Balanced third-order spherical aberration means that an appropriate amount of defocus has been added to minimize rms wavefront variance, as described in the eighth Zernike aberration polynomial. The pattern is wider as the spherical aberration spreads light to the edge of the irradiance pattern. In Figure 2c, -0.125 wave of balanced astigmatism, i.e., fourth Zernike polynomial, is introduced. The X-direction line

profile is shown as a solid line, while that in Y direction is shown as a dashed line. The line profile in Figure 2d has -1.0 waves of fifth-order balanced spherical aberration, i.e., a fifteenth Zernike coefficient of -0.1. The light is accumulated at the center by the fifth-order spherical and the balancing defocus while the balancing third-order spherical spreads light toward the edge. Consequently, a strong central peak and sidelobes are formed. Recall that the even aberration incident onto the detector lens is only half of that incident onto the disk. Thus, even if the focusing spot on the disk is well under the diffraction limit, the intensity pattern at the detector plane can be strongly modified.

We measured the wavefront at several planes with a LADITE laser-diode wavefront tester manufactured by WYKO Corporation. The objective lens was removed so that the entrance pupil of LADITE was located at the stop of the objective lens. The rms wavefront error was found to be 0.024λ and the Strehl Ratio was 0.985 as shown in Figure 3a. It was well collimated and diffraction limited[6].

We measured the PPBS separately. The objective lens was removed and a reference source was set in

the path of the reflected beam. The reference source was a laser diode source spatially filtered to be virtually aberration free. It was aligned and centered in the LADITE. This wavefront contained only aberration of the PPBS. We found that the PPBS had about 0.5 wave of astigmatism over the clear aperture.

The wavefront reflected from the disk was measured using the setup shown in Figure 1 with dashed lines. A high-quality first-surface mirror after the PPBS reflected the beam into a relay lens. The relay lens was used to relay the pupil of the objective lens to the entrance pupil of LADITE in order to avoid errors due to diffraction propagation. The relay lens consisted of two identical cemented doublets that form a 4f system, where the entrance and exit pupil of the relay lens was separated by four times the focal length of single lens. The relay lens was tested separately with the LADITE and exhibited only 0.012 wave rms aberration.

After data were acquired for the reflected wavefront after the PPBS, the wavefront of the PPBS was subtracted. This gives the wavefront before the PPBS that is due to a combination of laser optics and

objective/cover glass aberrations, as shown in Figure 3b. The aberration is mostly fifth-order spherical balanced with third-order spherical and defocus. The rms wavefront aberration is 0.054.

Recall that even aberrations are doubled in double pass. If the objective lens is well aligned, odd aberrations, like coma, are eliminated. The rms wavefront aberration focused down to the optical disk should be about half of the measured rms value of 0.054. This implies that the focused spot is definitely diffraction limited.

Reflected wavefronts after the PPBS are shown as 3D plot in Figure 3c and as X-profile in Figure 3d. The discrepancy between X and Y wave aberration fan is caused by the astigmatism of PPBS. The rms wavefront error is 0.079 wave, which is much worse than that before the PPBS. It is primarily a mixture of fifth-order spherical and astigmatism. Table I lists the first fifteen Zernike coefficients $Z_1(n)$ of the objective lens aberration and $Z_2(n)$ of the entire reflected wavefront. The first three polynomials, which represent tilt and defocus, are removed. As we discussed previously, the single-path aberration of the objective lens is half of the total, i.e., $Z_1/2$.

The aberration of the reflecting path includes contribution of objective lens $Z_1/2$ and beam splitter (Z_2-Z_1), the total is $(Z_2-Z_1/2)$.

A linear CCD array (CCD123 by Fairchild Weston Systems, 13μm by 10μm on 10μm pitch, dynamic range 5500:1) with 1728 elements was set in the detector plane to obtain line profiles of the irradiance pattern. Figure 4a shows the observed line profile. If no aberration were present, the edge should fall rapidly, as predicted in Figure 2a. However, a sidelobe shows up around a sharp central peak. Third-order aberration cannot produce this sidelobe and sharp central peak. The line profile was quite close to that predicted using fifth-order spherical aberration, as shown in Figure 2d. To model this line profile, we used the measured Zernike coefficients of Table I. Aberration of the objective before hitting the disk $(Z_1/2)$ is added in the entrance pupil of the objective, and aberration of the reflecting path $(Z_2-Z_1/2)$ is added in the exit pupil of the objective lens. The model was used to propagate the wavefront from objective lens down to the detector plane. The modeling result is shown in Figure 4b. A good agreement between modeled and measured beam profiles is achieved.

The Focusing Error Signal (FES) is generated from detector 2 using offset spot size method[2]. A typical FES vs defocus plot is shown in Figure 5. The solid line shows FES without aberration, while the dashed line shows FES with measured aberration. The aberrated FES has an offset at the center. The linearity of the aberrated FES is also changed significantly due to the presence of higher-order aberrations. The focus offset can produce a false focus. Nonlinearity decreases the performance of the servo system.

In conclusion, we reported an unexpected irradiance distribution in the detector plane of an optical data storage system. Through wavefront measurement and scalar diffraction modeling, we discovered that the energy redistribution was due to residual amounts of third-order and fifth-order spherical aberration of the objective lens and cover plate assembly. A significant amount of energy redistribution was observed, even though the beam was essentially diffraction limited.

The authors thank the Optical Data Storage Center at University of Arizona for financial support and WYKO Corporation for lending us LADITE

interferometer. We also wish to thank Steve Martinek of WYKO and Kevin J. Erwin of Optical Sciences Center for their technical support.

References

1. A.B. Marchant, Optical Recording, Addison-Wesley Publishing Co., New York, 1990, p. 8.

2. T.D. Milster, M.S. Wang, F.F. Froehlich, J.L. Kann, J.P. Treptau, and J.K. Erwin, "Differential Spot-Size Focus Servo", Proc. SPIE v. 1499 (1991).

3. J.P. Treptau, T.D. Milster, D.G. Flagello, "Laser Beam Modeling in Optical Storage Systems", Proc. SPIE v. 1415 (1991).

4. J.W. Goodman, Introduction To Fourier Optics, McGraw-Hill, Inc., 1968.

5. D.D. Cook, F.R. Nash, "Gain-induced guiding and astigmatic output of GaAs lasers", Journal of Applied Physics v. 46, no. 4 (1975).

6. F.F. Froehlich, M.S. Wang, and T.D. Milster, "Technique for simultaneous alignment and collimation of a laser diode in an optical data storage head", Appl. Opt. Vol. 30, No. 31 4481 (1991).

Tables

1. List of measured Zernike coefficients. $Z_1(n)$: aberration of the objective lens. $Z_2(n)$: Reflected wavefront.

n	$Z_1(n)$	$Z_2(n)$	n	$Z_1(n)$	$Z_2(n)$	n	$Z_1(n)$	$Z_2(n)$
1	0.000	0.000	6	0.008	-0.007	11	-0.019	-0.028
2	0.000	0.000	7	0.008	0.009	12	-0.014	-0.011
3	0.000	0.000	8	0.020	0.016	13	0.014	-0.001
4	0.032	0.143	9	-0.007	-0.014	14	0.033	0.031
5	0.021	0.036	10	-0.011	-0.007	15	-0.114	-0.111

Figure Captions

Figure 1. Optical system of a magneto-optical testbed. Testing path is drawn in dashed line.

Figure 2. Line profiles at detector plane when certain aberration is present: 2a. no aberration; 2b. -0.25 wave of spherical aberration; 2c. -0.125 wave of astigmatism in X (solid line) and Y (dashed line); 2d. -1.0 waves of fifth order spherical.

Figure 3. Measured wavefront. 3a. at objective lens; 3b. at objective lens, before PPBS; 3c. three dimensional wavefront, after PPBS; 3d. after PPBS in X direction.

Figure 4. 4a. Line profile at detector plane by a linear CCD array; 4b. prediction by using measured Zernike coefficients. Solid line: X direction. Dashed line: Y direction.

Figure 5. Calculated Focusing Error Signal (FES), solid line: without aberration; dashed line: with measured aberration.

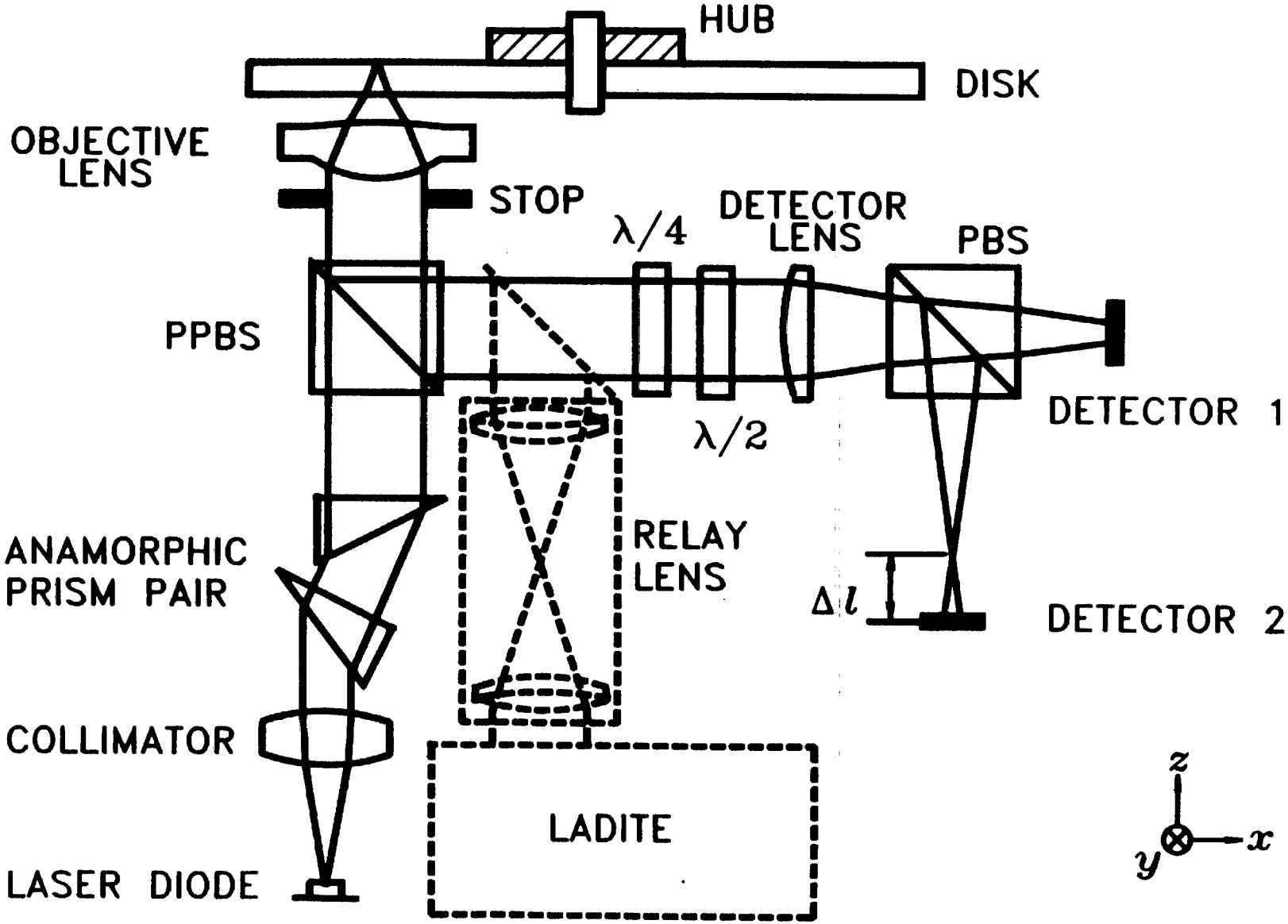
HUB
DISK
OBJECTIVE LENS
STOP
λ/4
DETECTOR LENS
PBS
PPBS
DETECTOR 1
λ/2
ANAMORPHIC PRISM PAIR
RELAY LENS
Δl
DETECTOR 2
COLLIMATOR
LADITE
LASER DIODE
z
y
x

Figure 1.

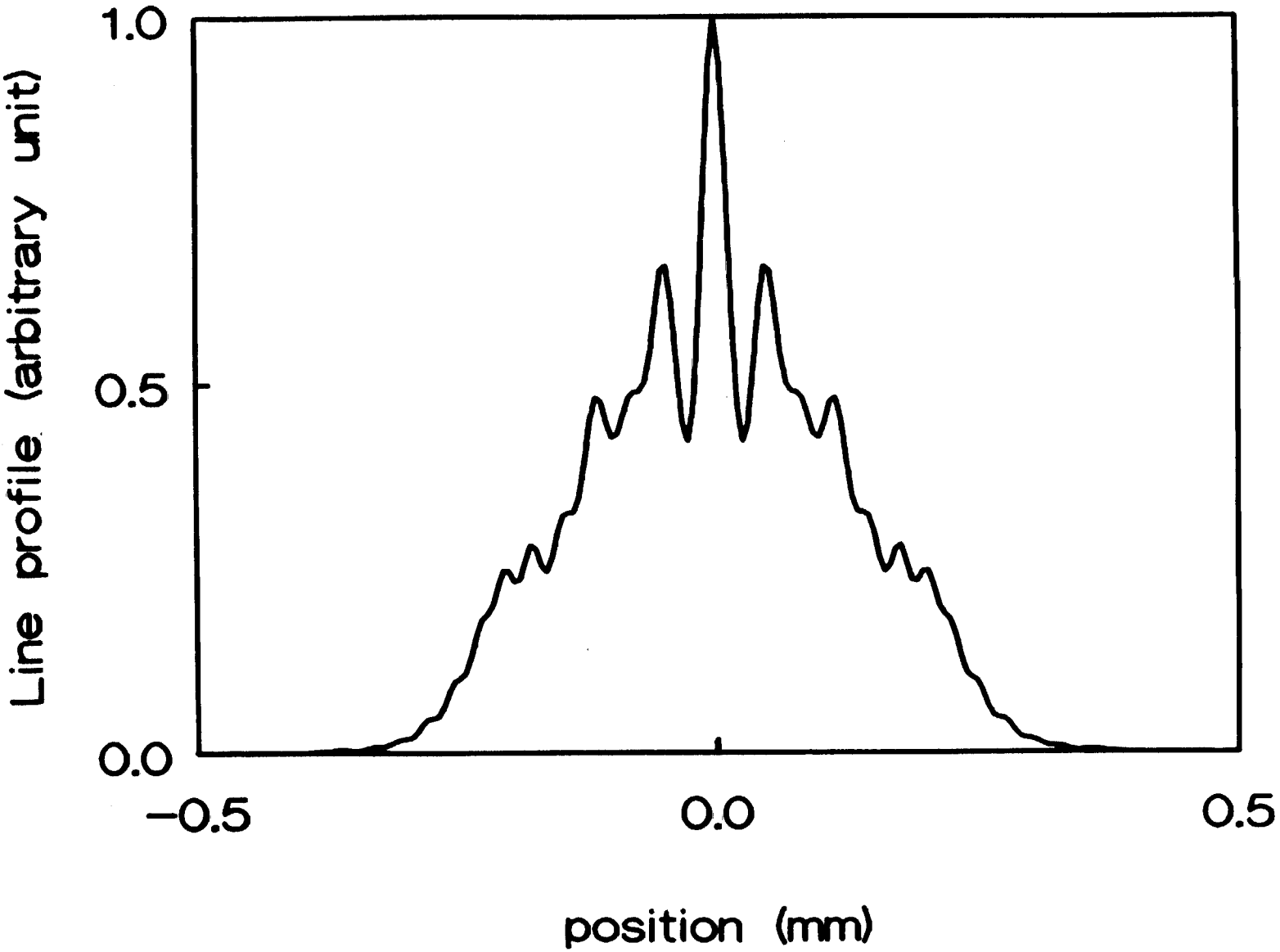

Figure 2a.

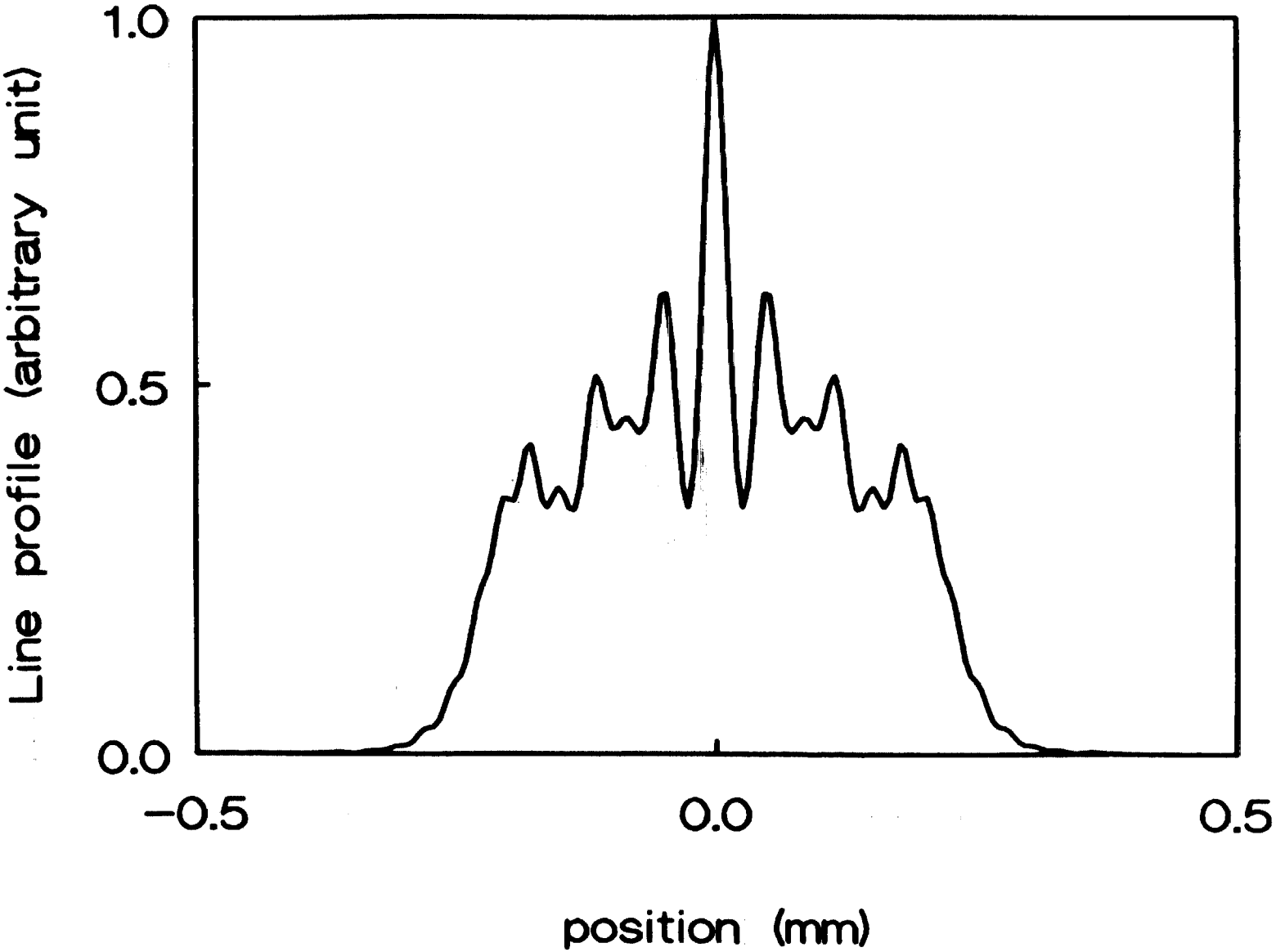

Figure 2b.

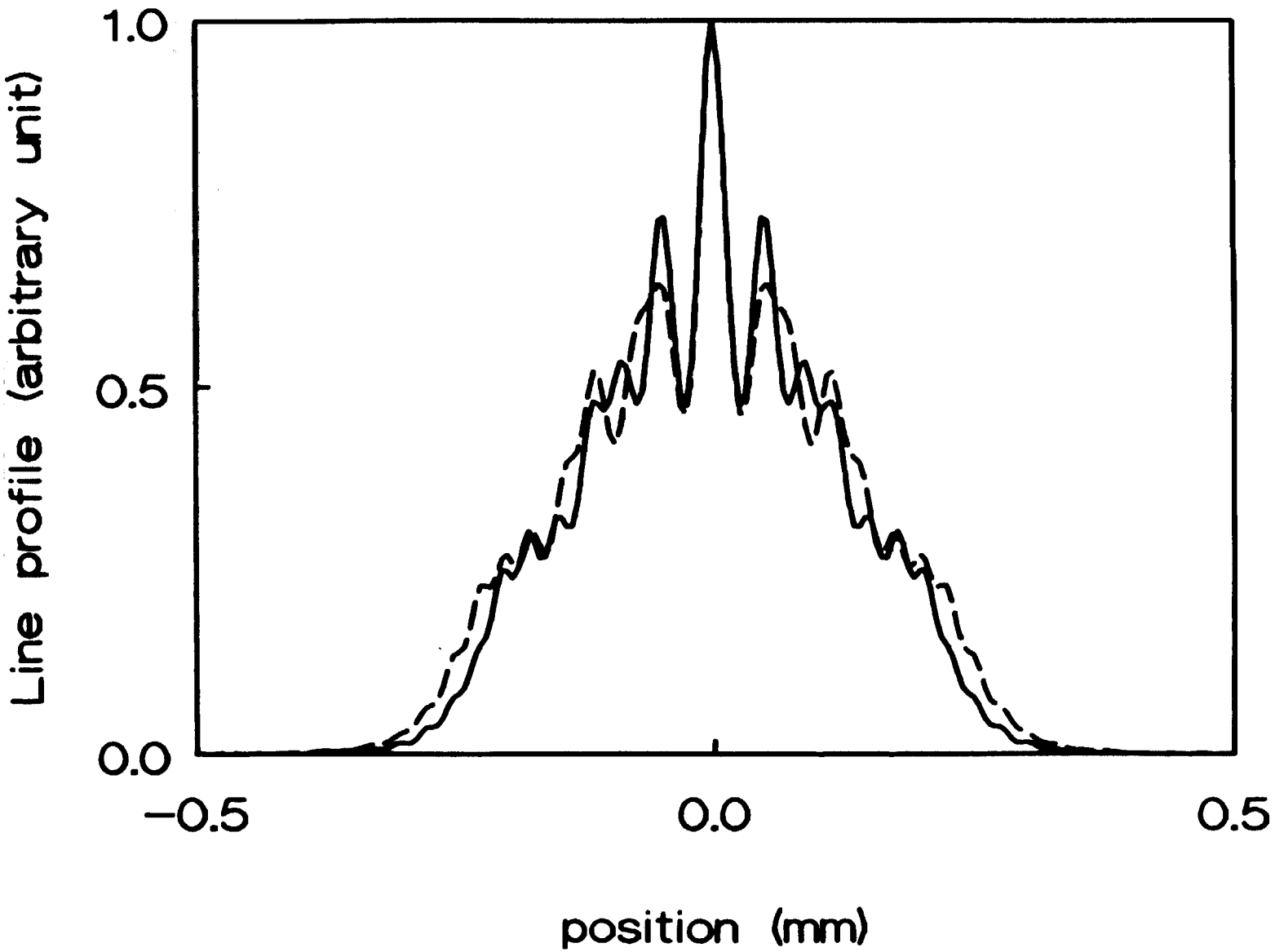

Figure 2c.

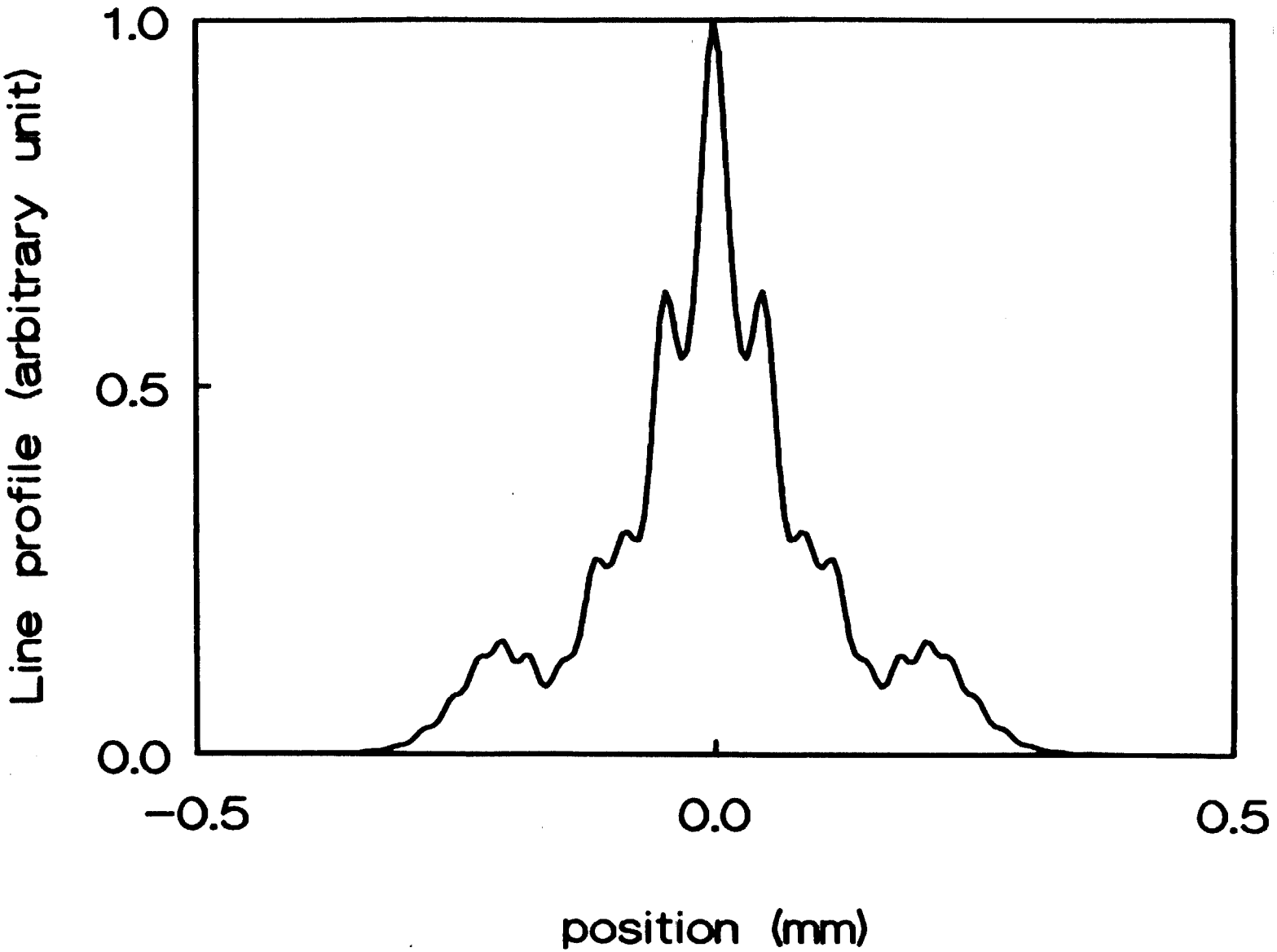

Figure 2d.

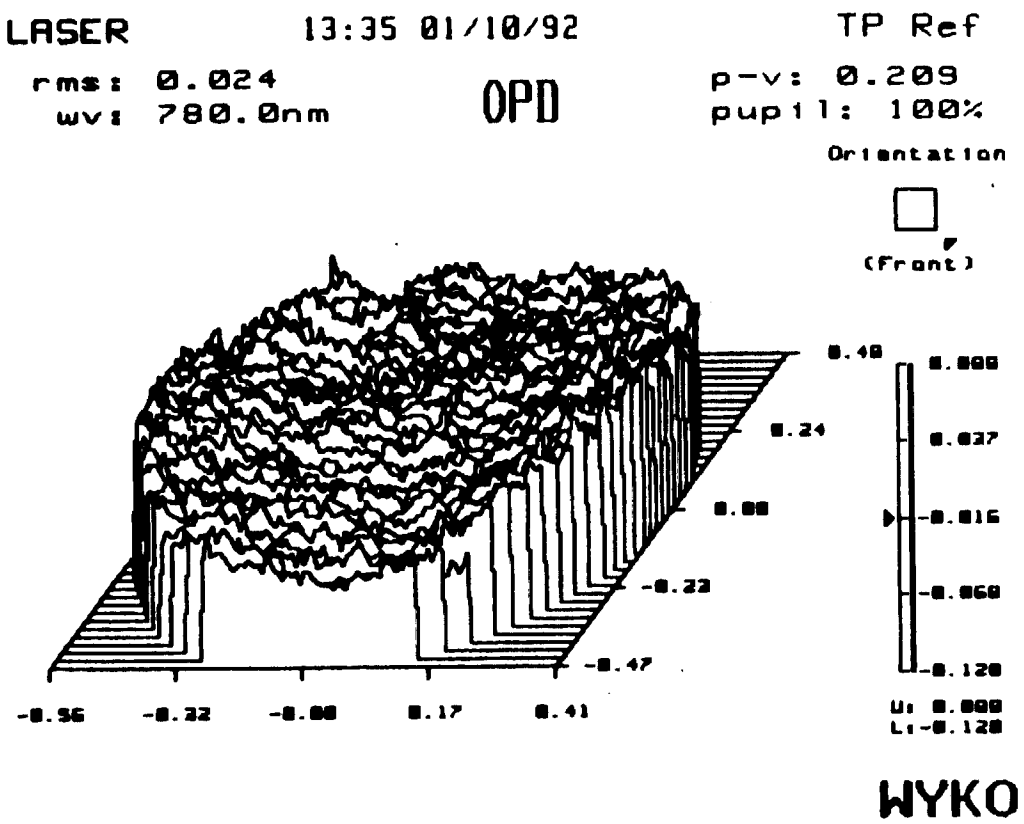

Figure 3a.

M. Wang
Optics Letters

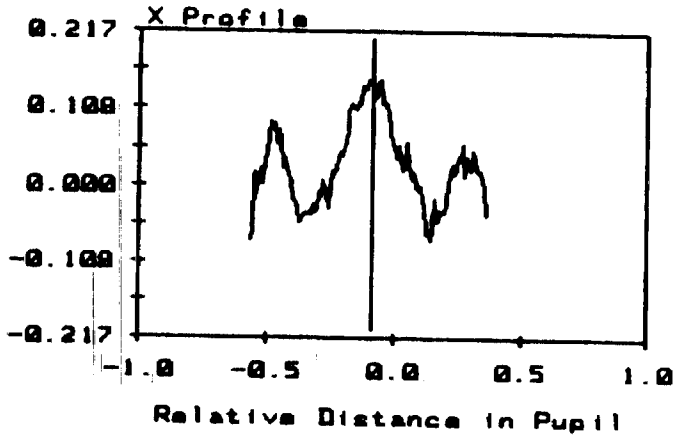
X Profile
0.217
0.108
0.000
-0.108
-0.217
-1.0
-0.5
0.0
0.5
1.0
Relative Distance in Pupil

Figure 3b.

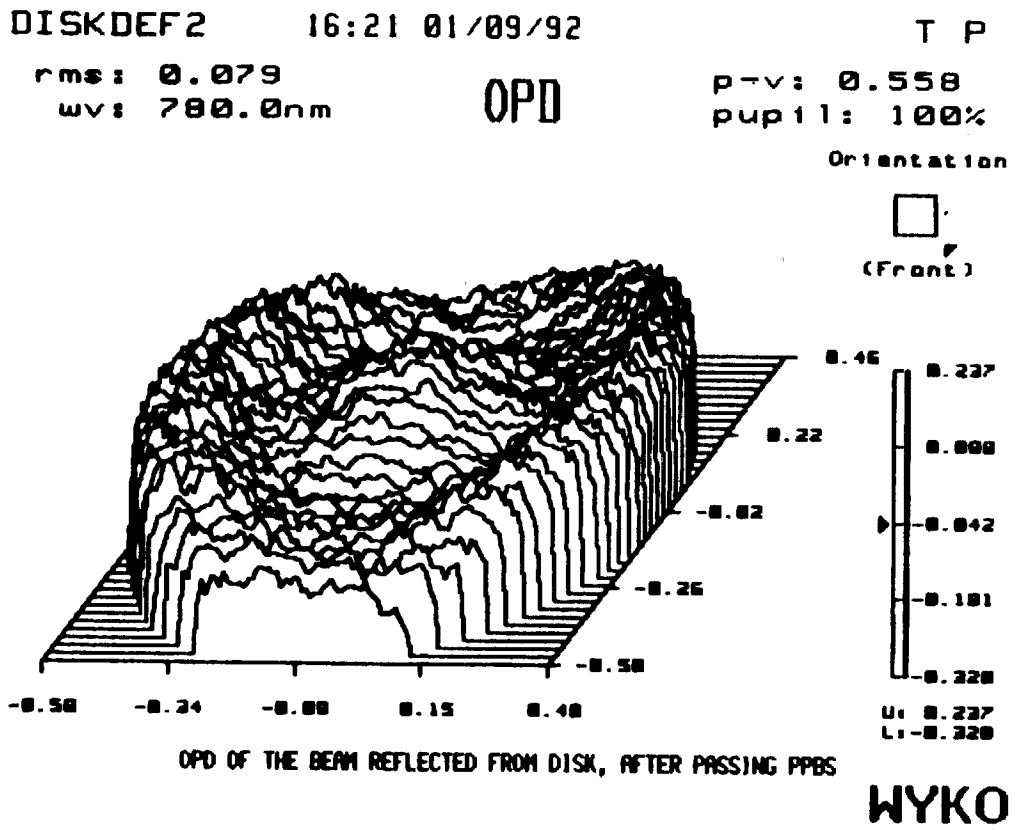

Figure 3c.

M. Wang
Optics Letters

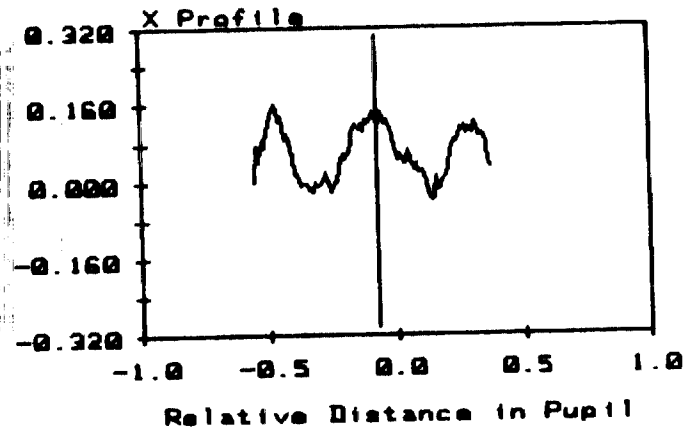

Figure 3d.

M.Wang
Optics Letters

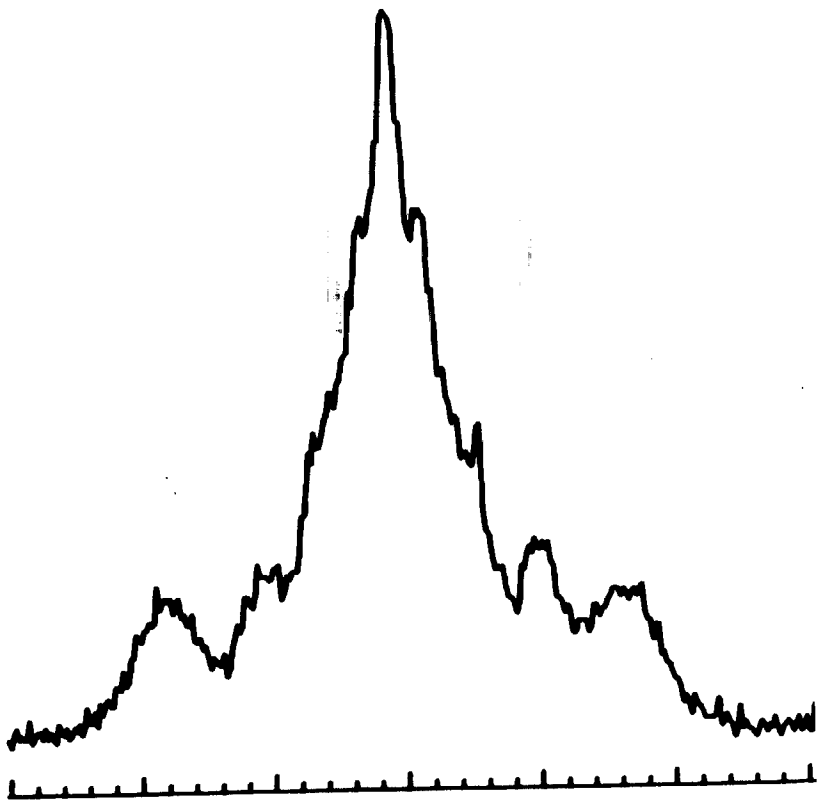

Figure 4a.

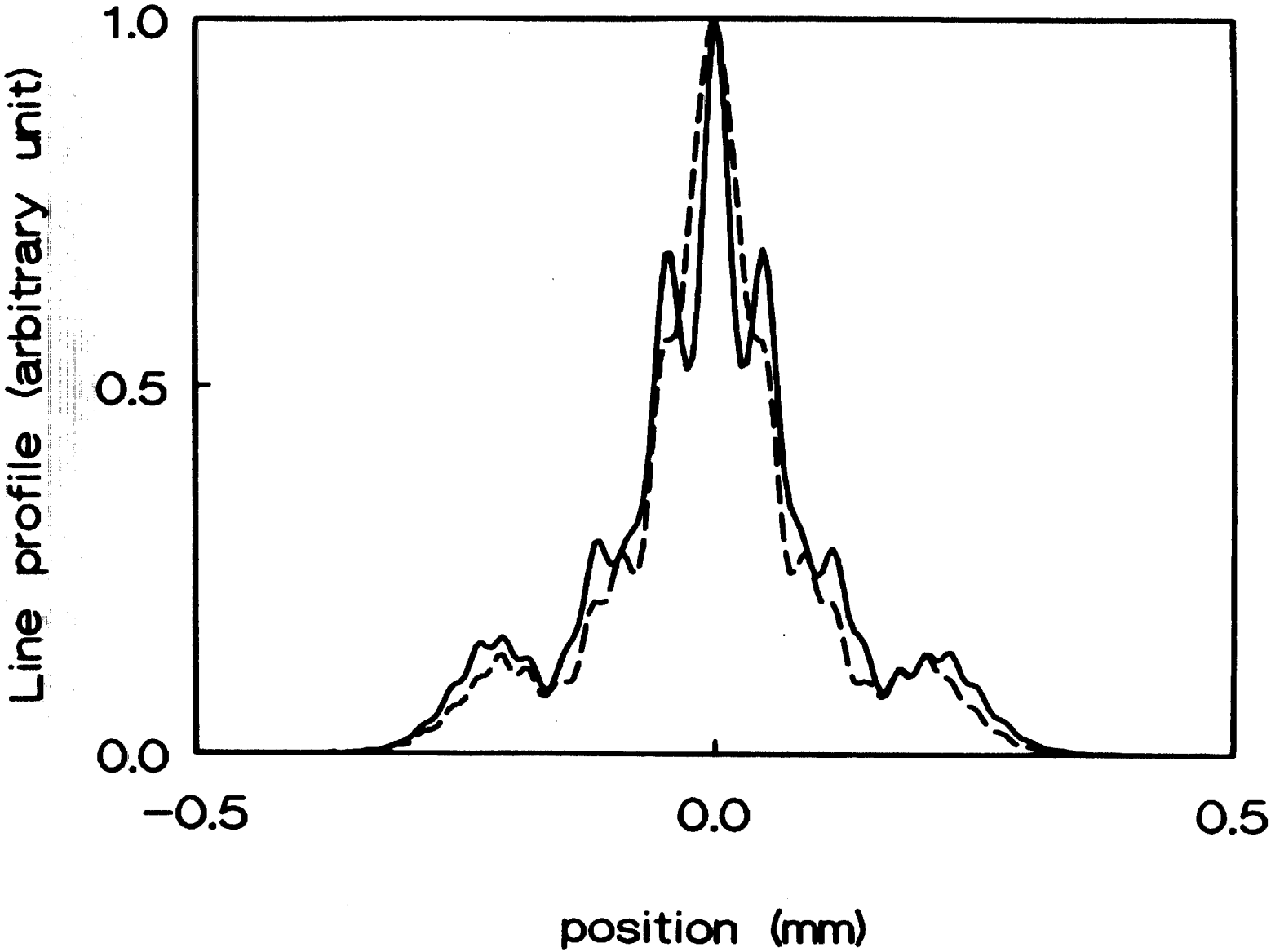

Figure 4b.

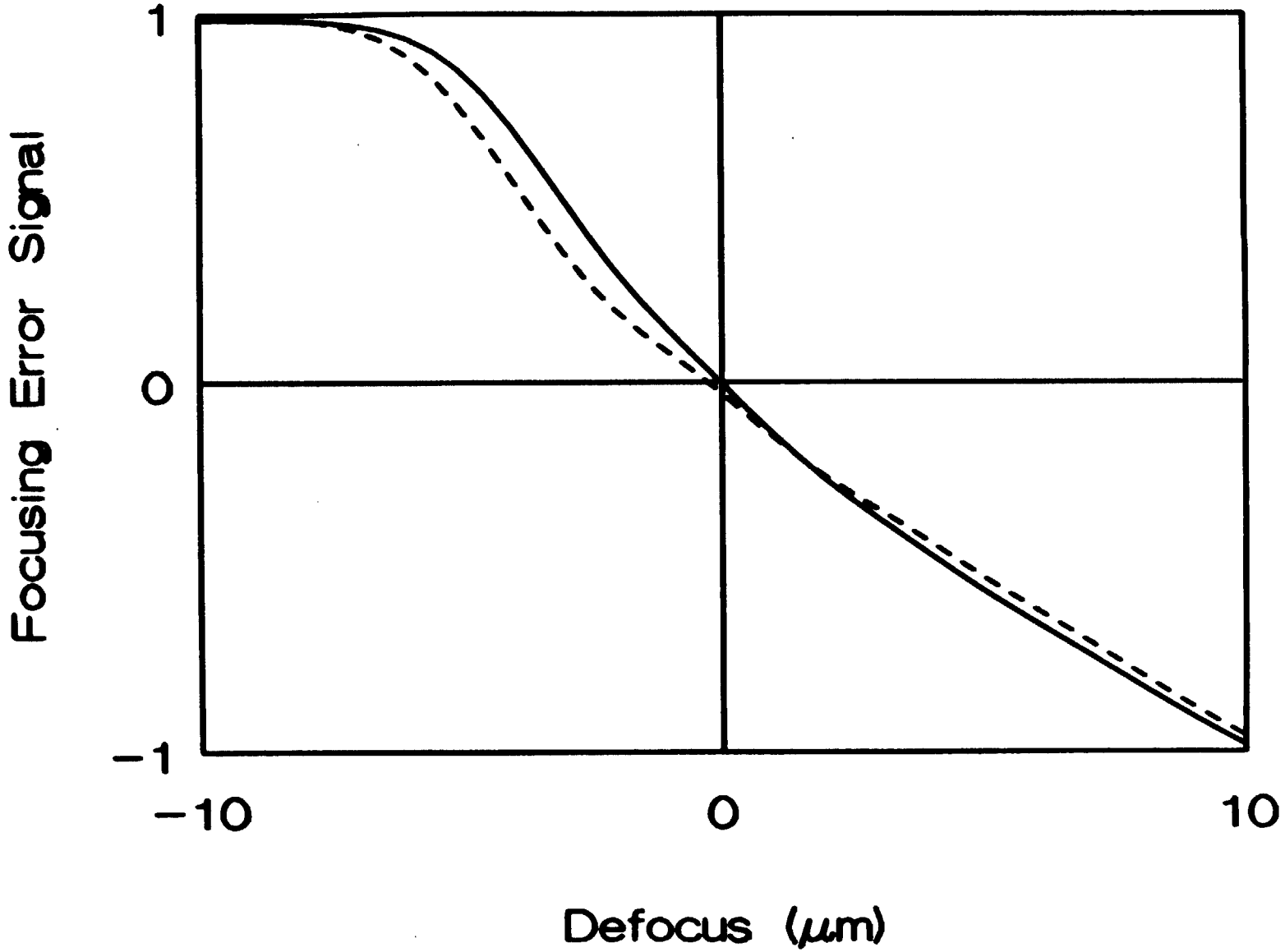

Figure 5.

APPENDIX K

PRECEDING PAGE BLANK NOT FILMED